Tuning the dimensionality of the heavy fermion compound $CeIn_3$

H. Shishido[1,2], T. Shibauchi[1], K. Yasu[1], T. Kato[1], H. Kontani[3],
T. Terashima[2], Y. Matsuda[1]

[1]*Department of Physics, Kyoto University, Kyoto 606-8502, Japan*
[2]*Research Center for Low Temperature and Materials Sciences, Kyoto University, Kyoto 606-8501, Japan*
[3]*Department of Physics, Nagoya University, Nagoya 464-8602, Japan*

Condensed matter systems that are both low dimensional and strongly interacting often exhibit unusual electronic properties. Strongly correlated electrons with greatly enhanced effective mass are present in heavy fermion compounds, whose electronic structure is essentially three-dimensional. We experimentally realize a two-dimensional heavy fermion system, adjusting the dimensionality in a controllable fashion. Artificial superlattices of antiferromagnetic heavy fermion compound $CeIn_3$ and conventional metal $LaIn_3$ are grown epitaxially. By reducing the $CeIn_3$-layer thickness, the magnetic order is suppressed and the effective electron mass is further enhanced. Heavy fermions confined to two dimensions display striking deviations from the standard Fermi liquid low-temperature electronic properties, associated with the dimensional tuning of quantum criticality.

Heavy fermion materials are metallic compounds with an extremely large effective electron mass, typically containing a rare-earth element. In these materials, the electrons populating the 4*f*-orbitals are, at high temperatures, essentially localized with well-defined magnetic moments. As the temperature is lowered, the localized moments are screened by conduction electrons (*s*,*p*,*d*-orbitals), forming a nonmagnetic state by virtue of the Kondo effect (*1*). At yet lower temperatures, the *f*-electrons dressed by conduction electron clouds (Kondo-cloud) become itinerant, forming a very narrow conduction band characterized by a heavy effective 'quasiparticle' mass. On the other hand, the Ruderman-Kittel-Kasuya-Yosida (RKKY) interaction, an intersite exchange interaction between the localized *f*-moments, promotes magnetic ordering. Thus the ground state of these compounds is either a nonmagnetic metal or a magnetically ordered state, as determined by the competition of the above two effects. Generally, in reduced spatial dimensions, many-body correlation effects due to the Coulomb interaction between electrons become more relevant. Moreover, thermal and quantum fluctuations are significantly enhanced, extending critical regimes with no long-range ordering to a wide temperature range. Therefore, many-body effects not observed in three dimensions are expected to arise in two-dimensional (2D) heavy fermion systems.

Quantum criticality is a central research issue in the physics of highly correlated matter (*2*,*3*). In conventional metals, interacting electrons (quasiparticles) are well described by Landau's Fermi liquid theory. Near the quantum critical point (QCP), where a second order phase transition occurs at zero temperature, low-lying spin-fluctuations give rise to a serious modification of the quasiparticle mass and the scattering cross section of the Fermi liquid. This results in a strong deviation of physical properties from the standard Fermi-liquid behavior. In heavy fermion metals, quantum criticality can be tuned by external parameters, such as doping, pressure and magnetic fields (*2*). Fabricating superlattice heterostructure provides another way to control the quantum criticality through `dimensional tuning'; however, the epitaxial growth of heavy fermion thin films has been a challenging issue (*4*-*6*).

There have been attempts to realize heavy fermion systems having low dimensions. One is the bulk crystals of Ce*T*In$_5$ (*T*=Rh, Co, or Ir), whose crystal structure yields alternating layers of CeIn$_3$ and *T*In$_2$ (*7*,*8*). However, the largely corrugated Fermi surface (*9*), small anisotropy of upper critical fields (*10*), and strong deviations from 2D antiferromagnetic spin fluctuations (*11*), all indicate that the electronic and magnetic properties of Ce*T*In$_5$ are anisotropic 3D rather than 2D. Another example is the bilayer 2D films of ^{3}He fluid (*12*), where the mass enhancement is observed near a QCP. Here the controlled parameter is the ^{3}He density of the second layer. However, the dimensional tuning from 3D to 2D heavy fermions is still lacking.

The heavy fermion compound $CeIn_3$ appears to be a good candidate for addressing the key issues of QCP physics. Bulk cubic $CeIn_3$ exhibits a three-dimensional antiferromagnetic ordering at T_N=10 K (*13,14*), which is destroyed in a quantum phase transition accessed by applying pressure. Near the critical pressure of p_c~24 kbar, in the vicinity of the QCP, $CeIn_3$ undergoes a transition into an unconventional superconducting state and a remarkable deviation from the Fermi-liquid behavior is reported (*14-16*). To adjust the dimensionality in a controllable way, we used molecular beam epitaxy (MBE) to grow the $CeIn_3$/$LaIn_3$ superlattices (Fig. 1A): m-layers of $CeIn_3$ and n-layers of isomorphic $LaIn_3$ were grown alternately, forming an "(m:n)" heterostructure. The clearly observed streak pattern of the reflection-high-energy-electron-diffraction (RHEED) (Fig. 1B) indicates the epitaxial growth of each layer with atomic-scale flatness. The cross-sectional transmission-electron-microscope (TEM) image (Fig. 1C, lower panel), showing bright spots corresponding to Ce atoms, demonstrates that the $CeIn_3$ layers are continuous even for the m=1 structures (*17*). The electron diffraction pattern with clear superspots (Fig. 1C, upper panel), the X-ray diffraction pattern (Fig. 1D) and the simulation results (Fig. 1E) all demonstrate the realization of an epitaxial superlattice structure. These indicate the successful confinement of f-electrons to the 2D spaces.

We investigate the transport properties of the (m:4) superlattices by varying m. Since the RKKY interaction decays as $1/r^3$, where r is the distance between the interacting magnetic moments, the magnetic interaction between the Ce-ions in different layers reduces to less than 1% of that between the neighboring Ce-ions within the same layer. Therefore the interlayer magnetic interactions are negligible. Resistivity ρ of the superlattices at room temperature is of the same order as for $CeIn_3$ (Fig. 2B, inset). $CeIn_3$ exhibits a $\rho(T)$ behavior typical of heavy fermion compounds. Below ~200 K, $\rho(T)$ increases due to the Kondo scattering and shows a maximum at T_{peak}~50 K. At T_N=10 K, $\rho(T)$ shows a distinct cusp, below which it decreases rapidly as the magnetic scattering is suppressed. In the superlattices, the hump structure of $\rho(T)$ at T_{peak}~50 K becomes less pronounced with decreasing m (Fig. 2A). Below T_{peak}, $\rho(T)$ increases again with decreasing temperature. Such behavior is caused by the interplay of the Kondo interaction with the crystal field effect (*18*), whose energy scale is 123 K in $CeIn_3$ (*19*). At lower temperatures, $\rho(T)$ shows a pronounced peak structure indicated by arrows for m=8, 6 and 3 (Fig. 2B). For m=2 and 1, $\rho(T)$ decreases gradually without exhibiting a pronounced peak below a characteristic temperature T_{coh}~1.6 K which marks the onset of coherent electron conduction.

The residual resistivity ρ_0 of the superlattices is larger than that of $CeIn_3$ (Fig. 2A). This is likely due to the inevitable scattering at the interfaces between the $CeIn_3$ and $LaIn_3$ layers, where Kondo holes by possible Ce/La disorder act as strong impurity scattering centers. We also note that the residual resistivity in the 2D planes can be enhanced with small impurity concentration by quantum fluctuations via enlarged effective cross section of local impurity scattering (*20*,*21*).

Next we discuss the magnetotransport. The observed distinct anisotropy in the magnetoresistance (Fig. 3A) indicates the substantial contribution from the 2D electrons confined within the layers, in sharp contrast to the 3D isotropic $Ce(La)In_3$. The negative magnetoresistance (Fig. 3A, inset) is consistent with the view that antiferromagnetic fluctuations responsible for the scattering can be suppressed by the magnetic field. The Hall coefficient $R_H(T)$ exhibits a cusp-like minimum in $CeIn_3$ and m=8, 6, and 3 (Fig. 3B). These cusp temperatures coincide with the temperatures at which $\rho(T)$ exhibit cusps (Fig. 2B, arrows). Therefore, we surmise that the observed transport anomalies for m=8, 6, and 3 appear as a result of magnetic ordering, as in $CeIn_3$. The low temperature behavior of the transport properties for m=2 and 1 are essentially different from those for $m>2$. For $m\leq 2$, $\rho(T)$ does not exhibit a pronounced peak and $R_H(T)$ decreases monotonically with decreasing temperature without showing the upturn. These results indicate that the magnetic order is suppressed with decreasing the $CeIn_3$ layer thickness and is vanishing near m=2. This conclusion is reinforced by Fig. 4A which shows that T_N decreases nearly linearly with $1/m$ and goes to zero in the vicinity of m=2. Therefore it is natural to conclude that the enhanced antiferromagnetic fluctuations associated with two-dimensionality are responsible for destroying the magnetic order.

The vanishing magnetic order implies the occurrence of a quantum phase transition close to m=2. Close to a QCP, the resistivity strongly deviates from the Fermi-liquid behavior $\rho(T)=\rho_0+AT^\alpha$ with α=2, where A is the Fermi-liquid coefficient. In Fig. 4B, the exponent α is mapped in the T vs $1/m$ diagram. The T^2-dependence is observed at low temperatures for $m>2$. In contrast, for m=2 a marked deviation from such behavior is observed (Fig. 4C): a T-linear dependence with $\alpha=1.01\pm0.02$ is seen below ~1/2 of T_{coh}, which corresponds to the Fermi temperature of heavy fermions. At even lower temperatures below ~140 mK, $\rho(T)$ shows a faster than linear decrease, which is suppressed by small magnetic fields (Fig. 4C, upper inset). We conclude that for m=2 the lowered dimensionality suppresses the magnetic order down to T_N~140 mK, which can be further suppressed by a small field (*17*). The T-linear behavior is consistent with scattering by the 2D antiferromagnetic fluctuations (*22*) enhanced by the QCP. This is in contrast to the 3D case, where α=3/2 is expected (*22*), and indeed α~1.6

is observed near the pressure-induced QCP in the bulk $CeIn_3$ (*14,15*).

Even for $m>2$ where the T^2-behavior is observed, the initial slope of $\rho-\rho_0$ at $T\rightarrow 0$ K becomes larger with decreasing m, and A is enhanced toward $m=2$ (Fig. 4A). Because A is related to the Sommerfeld coefficient of specific heat γ as $A=a_0\gamma^2$, with a_0 close to the universal value of 10^{-5} $\mu\Omega$ cm (K mol/mJ)^2 (*14,21*), the large A immediately indicates the enhanced quasiparticle mass. At low temperatures below ~1 K the resistivity of $LaIn_3$ is much smaller than that of superlattices and its temperature dependence is negligible. Thus the observed large A values indicate that the temperature dependent part of the resistivity is governed by the 2D heavy fermion layers. In fact, the γ-value estimated from A is enhanced from the bulk $CeIn_3$ value of ~120 mJ/K^{2}mol and reaches ~350 mJ/K^{2}mol for $m=3$, which corresponds to the quasiparticle mass at least several hundreds times larger than the free electron mass. Because the T-linear behavior observed for $m=2$ suggests further enhancement of A, it is tempting to associate this result with diverging quasiparticle mass due to the quantum fluctuations enhanced upon approaching a QCP. For $m=1$ the determination of A is ambiguous because of the weak temperature dependence of ρ. We note that the diverging behavior of γ near a QCP is also reported in bilayer films of ^{3}He systems (*12*).

Quantum criticality is reported to be strongly modified by magnetic fields in strongly correlated electron systems (*2,9,23,24*). As shown in the lower inset of Fig. 4C, the quantum criticality for $m=2$ is removed by strong magnetic fields and the Fermi-liquid properties with $\alpha=2$ are recovered. Simultaneously, the A value is quickly suppressed with H (Fig. 4A). Thus both temperature and field dependencies of the transport properties provide strong support for the presence of the quantum phase transition in the vicinity of $m=2$, which is tuned by the “dimensionality” parameter. The successful growth of epitaxial Ce-based superlattices promises to provide a setting to explore the fundamental physics of strongly correlated electron systems such as 2D Kondo lattice and, potentially, 2D superconductivity near a QCP.

REFERENCES

1. A. C. Hewson, *The Kondo problem to heavy Fermions* (Cambridge University Press, Cambridge, UK, 2003).

2. P. Gegenwart, Q. Si, F. Steglich, *Nature Phys*. **4,** 186 (2008).

3. S. Sachdev, *Quantum Phase Transition* (Cambridge University Press, Cambridge, UK, 2000).

4. M. Jourdan, M. Huth, H. Adrian, *Nature* **398**, 47 (1998).

5. D. Groten, G. J. C. van Baarle, J. Aarts, G. J. Nieuwenhuys, J. A. Mydosh, *Phys. Rev. B* **64**, 144425 (2001).

6. M. Izaki *et al., Appl. Phys. Lett.* **91**, 122507 (2007).

7. H. Hegger *et al., Phys. Rev. Lett.* **84**, 4986 (2000).

8. C. Petrovic *et al*., *J. Phys.: Cond. Matt.* **13**, L337 (2001).

9. H. Shishido, R. Settai, H. Harima, Y. Onuki, *J. Phys. Soc. Jpn.* **74**, 1103 (2005).

10. Y. Ida, R. Settai, Y. Ota, F. Honda, Y. Onuki, *J. Phys. Soc. Jpn.* **77**, 084708 (2008).

11. G.-q. Zheng *et al., Phys. Rev. Lett.* **86**, 4664 (2001).

12. M. Neumann, J. Nyeki, B. Cowan, J. Saunders, *Science* **317**, 1356 (2007).

13. J. M. Lawrence, S. M. Shapiro, *Phys. Rev. B* **22,** 4379 (1980).

14. N. D. Mathur *et al., Nature* **394,** 39 (1998).

15. G. Knebel, D. Braithwaite, P. C. Canfield, G. Lapertot, J. Flouquet, *Phys. Rev. B* **65,** 024425 (2002).

16. S. Kawasaki *et al*., *J. Phys. Soc. Jpn.* **73**, 1647 (2004).

17. See supporting material on *Science* Online.

18. S. Kashiba, S. Maekawa, S. Takahashi, M. Tachiki, *J. Phys. Soc. Jpn.* 55 1341 (1986).

19. W. Knafo *et al.*, *J. Phys.: Cond. Matt.* **15**, 3741 (2003).

20. Y. Nakajima *et al.*, *J. Phys. Soc. Jpn.* **76**, 024703 (2007).

21. H. Kontani, *Rep. Prog. Phys.* **71**, 026501 (2008).

22. T. Moriya, K. Ueda, *Adv. Phys.* **49**, 555 (2000).

23. A. Bianchi, R. Movshovich, I. Vekhter, P. G. Pagliuso, J. L. Sarrao, *Phys. Rev. Lett.* **91**, 257001 (2003).

24. T. Shibauchi *et al.*, *Proc. Natl. Acad. Sci. USA* **105**, 7120 (2008).

25. E. E. Fullerton, I. K. Schuller, H. Vanderstraeten, Y. Bruynseraede, *Phys. Rev. B* **45**, 9292 (1992).

26. We thank M. Izaki, N. Kawakami, H. Kurata, K. Miyake, and A. Tanaka for discussion. This work was supported by KAKENHI from JSPS and by Grant-in-Aid for the Global COE program ``The Next Generation of Physics, Spun from Universality and Emergence’’ from MEXT.

FIGURE LEGENDS

Figure 1: Superlattice heterostructure of $CeIn_3$ and $LaIn_3$. (**A**) Illustration of the artificial superlattice (m:n) composed of m(=1) unit cell thick layer of $CeIn_3$ and n(=3) layers of $LaIn_3$. (**B**) Streak patterns of the RHEED during the crystal growth. (**C**) Cross-sectional TEM image of (1:3) superlattice. Ce atoms can be identified as brighter spots than the La and In atoms (lower left). Diffraction pattern of electron beam incident along [110] direction (upper right). (**D**) X-ray reciprocal lattice mapping for the (8:4) superlattice. A satellite peak is observed around the fundamental (113) peak along the Q_{001} direction. (**E**) Diffraction patterns using monochromatized Cu $K_{\alpha 1}$ X-ray (black line) around the (002) main peaks of (m:4) superlattices for m=1, 2, 4, 8 with typical superlattice thickness of 200 nm. The step-model simulations (red line) which neglect interface and layer-thickness fluctuations (*25*) reproduce both the intensities and the positions of the satellite peaks (solid arrows). Some higher-order peaks are below the experimental resolutions (dotted arrows). Each curve is shifted vertically for clarity.

Figure 2: Temperature dependence of the resistivity in (m:4) superlattices for m=1 (green), 2 (red), 3 (blue), 6 (sky blue), and 8 (yellow). Each data set is normalized by its value at 10 K (**A**) and the maximum value $\rho_{\max}$ (arrows) at low temperatures (**B**) to compensate for the slight differences in resistivity at room temperature between the films (inset in **B**). The data for the 200 nm–thick $CeIn_3$ (blue square) and $LaIn_3$ thin films (black square) are also shown. $\rho(T)$ of $CeIn_3$ film coincides well with that of bulk single crystals.

Figure 3: Magnetotransport of the superlattices. (**A**) Transverse magnetoresistance $\Delta\rho(H)/\rho(H=0)$ of the (1:4) superlattice in magnetic field $\boldsymbol{H}$ rotated within the *ac*-plane at 0.6 K (red) and 4.5 K (blue). The current is applied along the *b*-axis. Here the *c*-axis is perpendicular to the layers. θ is the angle between $\boldsymbol{H}$ and the *c*-axis. The inset shows $\Delta\rho(H)/\rho(0)$ for $\boldsymbol{H}//c$ at several temperatures. (**B**) Temperature dependence of the Hall coefficient R_H for the superlattices and $CeIn_3$. $R_H(T)$ shows a cusp-like minimum (arrows) for m=8, 6, and 3 as well as $CeIn_3$.

Figure 4: Temperature vs dimensionality phase diagram. (**A**) Neel temperature T_N (red circles) and Fermi-liquid coefficient A as function of $1/m$ (open blue squares). For m=2, the A values are determined from $\rho(T)$ under magnetic fields (solid squares). The solid and dashed lines are guides for the eye. (**B**) Temperature and layer-thickness evolution

of the exponent α derived from the expression $\rho(T)=\rho_0+AT^{\alpha}$. (**C**) $\rho(T)$ at low temperatures for m=2. Solid line is a best fit to the T-linear dependence above T_N~140 mK. The upper inset displays $\rho(T)$ under small magnetic fields applied perpendicular to the film plane. The lower inset is a plot of $\rho-\rho_0$ vs T^2 at several fields. Solid lines are the fits to the T^2 dependence.

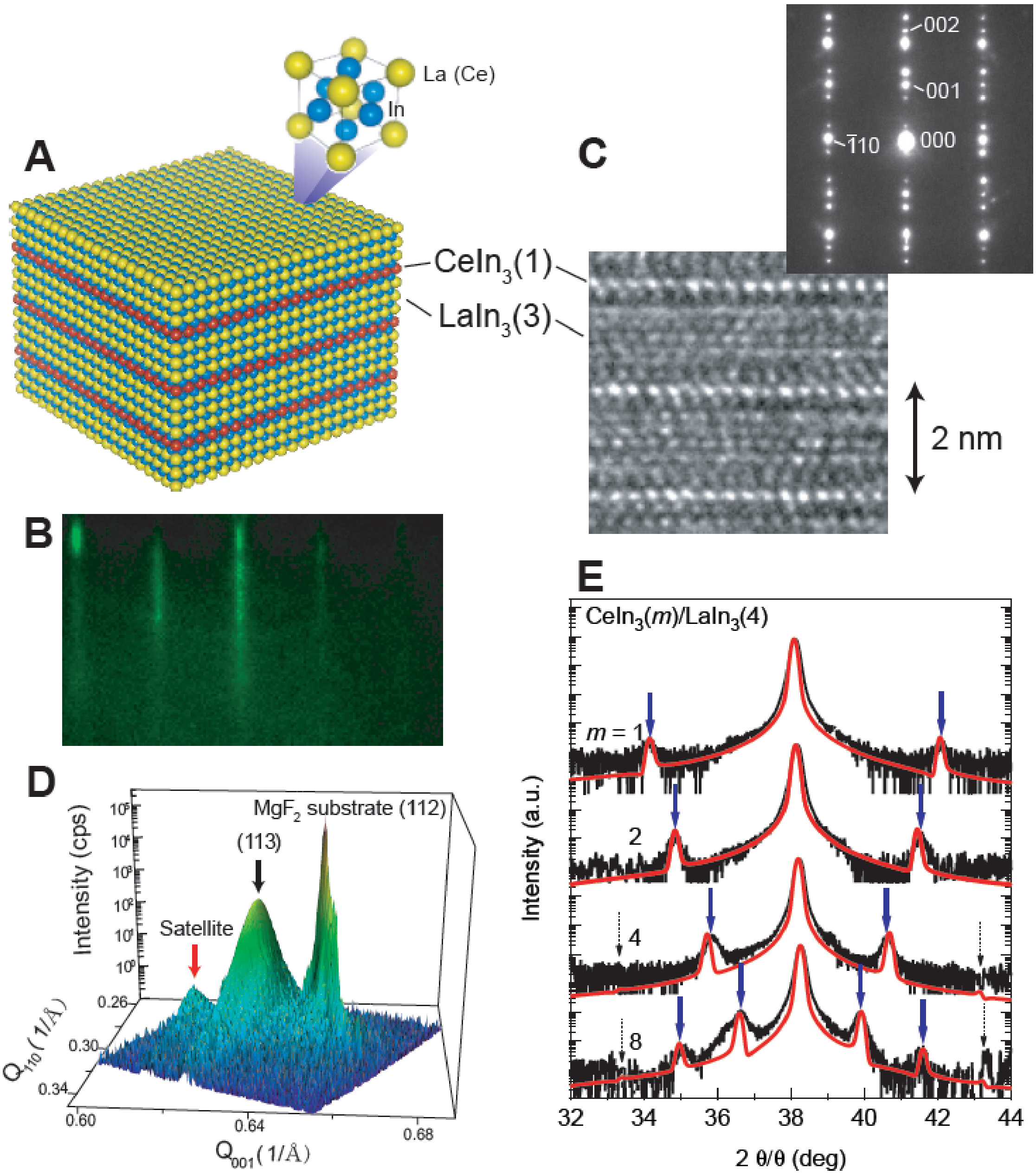

Fig. 1 Shishido *et al.*

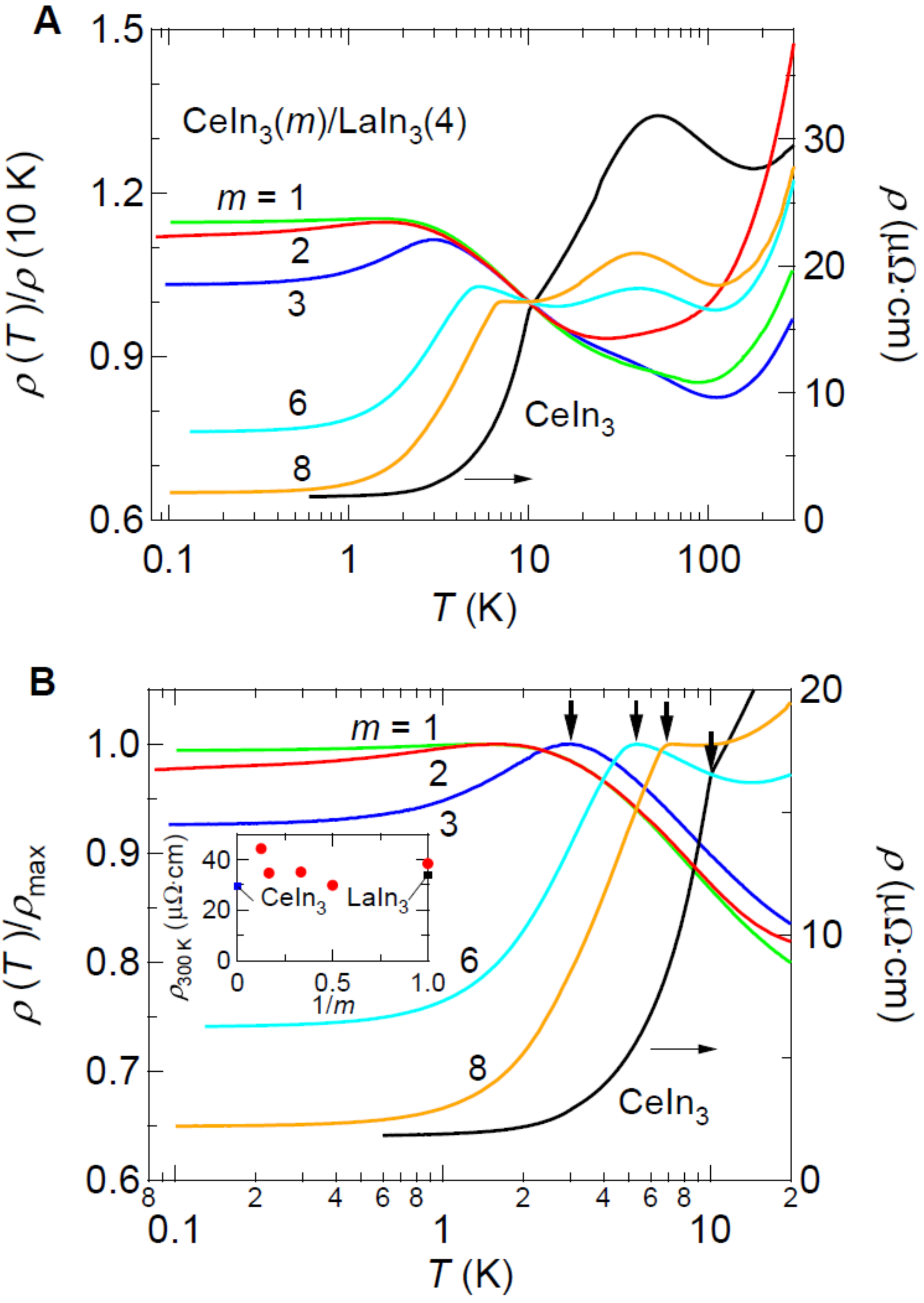

Fig. 2 Shishido *et al.*

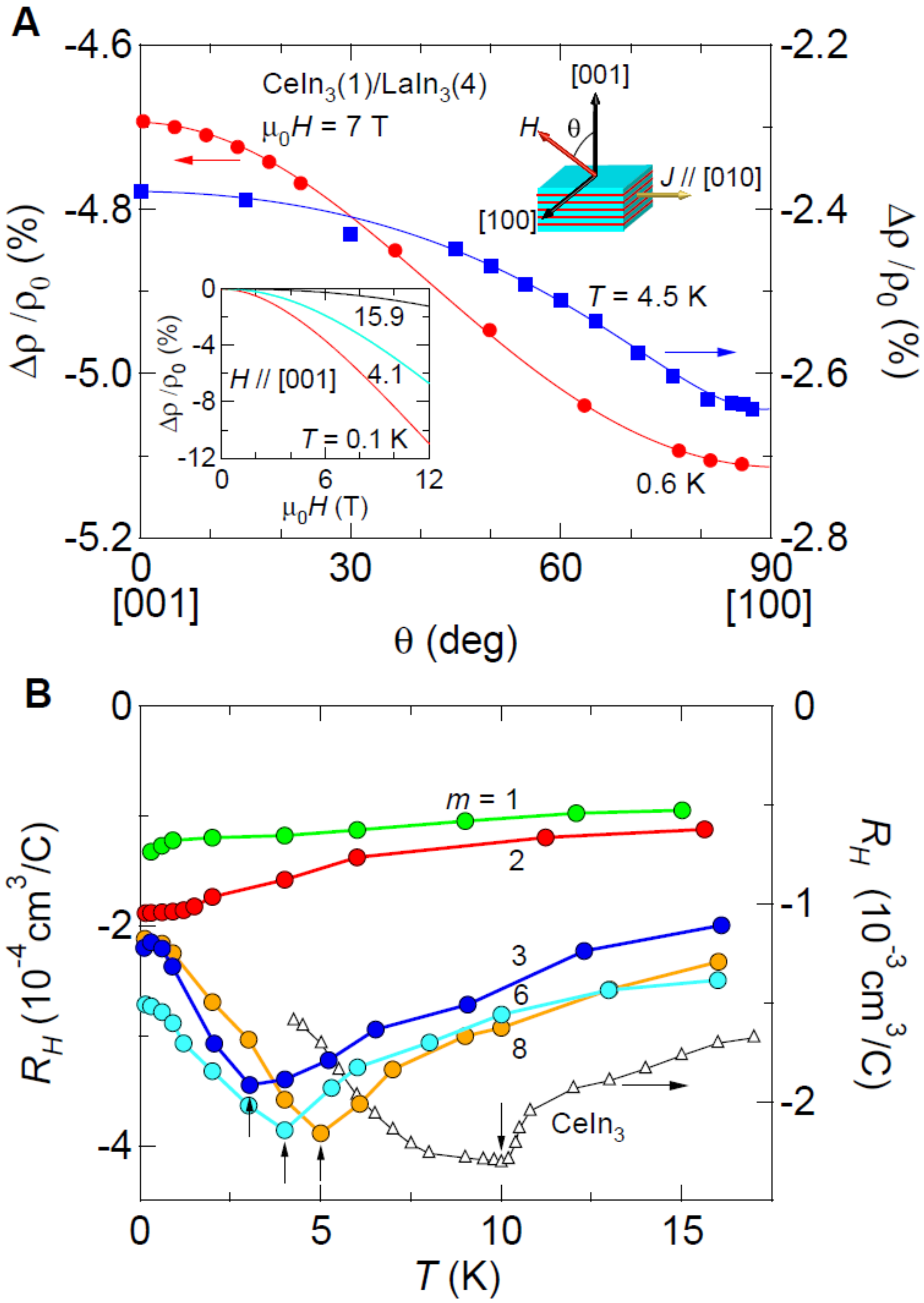

Fig. 3 Shishido *et al.*

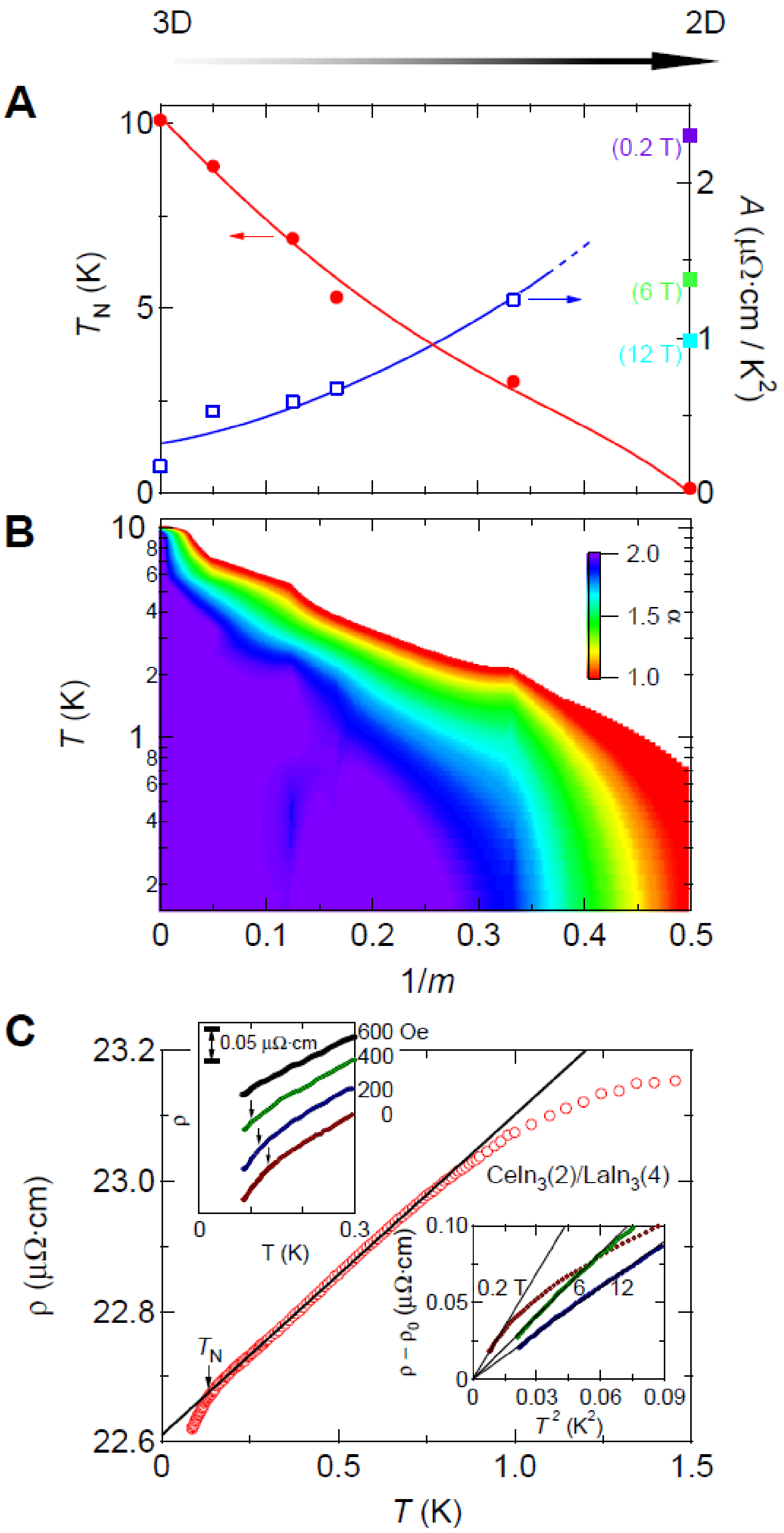

Fig. 4 Shishido *et al.*